Egypt. J. Chem. **Vol. 63,** No. 4, pp. 1269 - 1278 (2020)

Egyptian Journal of Chemistry
http://ejchem.journals.ekb.eg/

3D Porous Silicon (Nanorods Array, Nanosheets, and Nanoclusters) Production

Marwa Nabil[1,*], Kamal R. Mahmoud[2], Raghda Nomeir[3], EM El-Maghraby[3] and Hussien A. Motaweh[3]

[1] *Advanced Technology and New Materials Research Institute, City for Scientific Research and Technology Applications, New Borg El-Arab City, Alexandria, 21934, Egypt.*

[2] *Department of Physics, Faculty of Science, Kafrelsheikh University, Kafr El Sheikh, 33516, Egypt.*

[3] *Department of Physics, Faculty of Science, Damanhour University, Egypt.*

IN this research, using powder technology manufacturing is as a pioneering, low cost, a simple and safe method for the fabrication of nano-porous silicon (NPS-powder). It's attractive carriers for targeted in several research fields. It's prepared using a combination of alkali chemical etching process and ultra-sonication technique; through the utilization of commercial silicon powder; with high yield efficiency (81.43%). Several 3D-NPS-shapes (nanorods array, nanosheets, and nanoclusters) are fabricated. It's a mixture of microporous and mesoporous silicon powder {pore size (28-140 nm)}. The main factors which affect the production of NPS-powder are (KOHconc.), sonication time, separation process and drying velocity.

Keywords: Microporous materials, Chemical synthesis, X-ray diffraction.

Introduction

Nanoporous silicon (NPS) is very impressive for many kinds of experimental researches. It has a large specific surface area; in addition, it's easily produced [1]. Plus, its pore sizes and the surface chemistry are controllable [2]. NPS powder can be obtained using several techniques [3-5]; as electrochemical [6], vapor phase etching [7] and stain etching of Si-wafers [8]. The production of bulk (PS) in large dimensions shape that is synthesized using ball milling process and pressing, simultaneously, and sintering of Si-particles. As a competitive process for using electrochemical etching technique in HF [9]; (i) preparation of microspheres NPS powder using chemical vapor deposition for decomposition of disilane gas (Si_2H_6), (ii) synthesis of NPS powder starting with commercial Si powder using photo-thermal annealing in O_2-atmosphere [10]. Noticeable, the especial features of the stain-etching technique are the simplicity and the capability of producing large area of porous silicon. [11]

Recent researches have proved the capability of the ultra-sonication technique for synthesis of many materials [12, 13]. The wave motion is transferred from ultrasound source to the solution in a bubble shape. So, the bubbles grow fast and reach the unstable size. And, the energy is enhanced as a result of the bubbles collapse that leads to chemical effect [14]. The shock waves formation linked with the bubbles collapse that occurs during the ultrasonic irradiation of the solution. The acoustic cavitation produces the shock waves that increase the momentum of the particles. [15]

*Corresponding author e-mail: marwamoh2000@yahoo.com
Received 09/07/2019; Accepted 28/08/2019
DOI: 10.21608/ejchem.2019.14613.1885

As a result of the properties differentiation of NPS material than the properties of bulk material, NPS material is reckoned as the base of modern industries in many fields [16], such as metallurgy, electronics, and Photonics [10]. There are a large number of domains such as microelectronics, optoelectronics and chemical sensors [17]. The morphological features of NPS material, specific surface area and the pore wall size, are the key factors of the NPS performance. [18]

In this work, the combination of the alkali chemical etching process and the ultra-sonication technique is used as a new, low cost, safe and simple synthetic route for the NPS different constructions powder preparation starting by commercially available silicon powder. It is a very interesting way for producing bulk quantities with high yield efficiency of NPS-powder.

Materials and Methods

To prepare NPS-powder, it is started by commercially available Si-powder [Silicium, Pulver – 99 %, 7 gm). Fig. 1 presents the NPS powder synthesis using the combination of the anisotropic alkali chemical etching process and the ultra-sonication technique, (ULTRAsonik 208H, KSU-600) [19]. The commercial silicon powder was dispersed in the etching glass vessel which contains alkaline solution. The alkaline compound used was KOH of concentration range (3, 4.5 and 6 wt %) dissolved in ultrapure water [18MΩ deionized water]. n-propanol was added up to the degree to which it was miscible in aqueous solutions. n-propanol is used as a wetting agent of concentration 30 vol %. So, the glass vessel was exposed to the ultra-sonication waves for different times (2, 3, and 4 hr). The powder product is filtrated and washed, then dried overnight at 40°C to obtain NPS-powder.

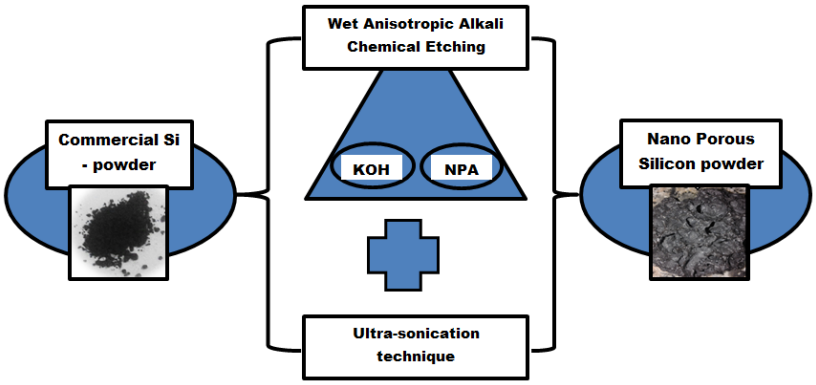

Fig. 1: Experimental illustration of the nano-porous silicon preparation

The structure and crystallization of the powder product are characterized by XRD (X-ray Ultra diffract-meter, using Cu-Kα radiation = 1.5405 Å at a scanning rate of 4° min^{-1}, 7000 Schimadzu diffract-meter). In addition, the crystallite size and the energy gap values of NPS can be calculated using XRD spectra. The composition of the deposited powders was explored elementary by JEOL 5300 scanning electron microscope embedded with EDAX microanalysis. An accelerating voltage of 20KV was used. FTIR (Fourier Transform Infrared Spectrophotometer- Shimadzu- 8400s, Japan) and Raman Spectroscopy (Senteral - Bruker Raman micro-spectroscopy, at excitation wavelength 330 cm^{-1}) are recording the chemical bonds of the NPS powder synthesis process. The NPS powder morphology is inspected using SEM {Scanning electron microscopy, JEOL (JSM 5300), at an accelerating voltage of 20 KV} and transmission electron microscope (TEM; JEOL, Japan),

Results and Discussion

The produced powders were NPS powder (5.7 gm) with a percentage of powder production reaches 81.43%, as shown in Fig. 1. The preparation mechanism for NPS powder is described. It starts with commercial Si powder suspended in KOH solution and n-propanol with different concentrations in the ultra-sonication unit at different times. The chemical mechanism equations of the NPS powder formation was illustrated in previous work. [20]

As a reference characterization technique for NPS powder product, XRD has chosen for the

analysis of the diffraction patterns. It can be very useful to study the changes of the crystal structure induced by the combining the wet alkali etching and ultra-sonication techniques, simultaneously [21]. XRD data describes the NPS diffraction patterns, as shown in Fig. 2. The changes in the peak intensities and peak positions are indicated, which depend on the size of NPS. It depends on several parameters; the sonication time, KOH_{conc} and the drying process of the NPS powder product. Fig. 2.a, b and c show the full width at half maximum (FWHM) of the peaks around 28.23°, 47.193°, 56.023°, 68.989°, 76.261°, 87.9382°, and 94.8370° (JCPDS Card No. 01-079-0613 and 00-027-1402) [20, 21], which correspond to (111), (220), (211), (400), (331), (422) and (511), respectively. In addition, the SiO_2 layer broad peak is recorded at 21.5° as that indicates the formation (SiO_2/Si), as shown in fig. 2.c.[22, 23]. The crystallites size of (Si) can be estimated from diffraction pattern analysis by measuring FWHM and applying Scherrer's equation. The energy band gap value confirms the formation of NPS that has a characteristic of the energy gap widening than in the case of nancrystalline silicon (n-Si). [2]

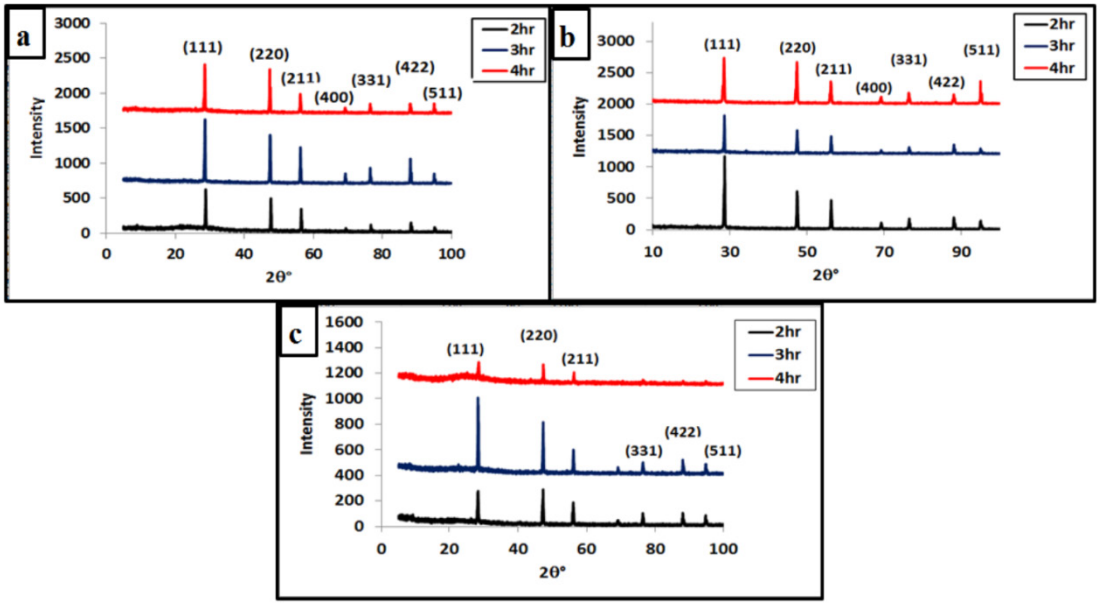

Fig. 2: XRD patterns of NPS powder using different ($KOH_{conc.}$) at several sonication times; (a) $KOH_{conc.}$ = 3 wt % at sonication time (2, 3 and 4hr), (b) $KOH_{conc.}$ = 4.5 wt % at sonication time (2, 3 and 4hr), and (c) $KOH_{conc.}$ = 6 wt % at sonication time (2, 3 and 4hr).

There are other important effective factors for the formation process of NPS powder, which are shown in the following; the 1st parameter is the drying process. Fig. 3.a presents the polycrystalline-NPS spectra that as a result of fast drying (using heat treatment). In addition, the broad spectra are corresponding to the oxide layer (SiO_2) presence, which surrounds the NPS-particles. At slow drying (without heat treatment); broad spectrum is appeared strongly than the other. Then, SiO_2 spectrum has appeared as a result of an NPS oxidation process during the exposure to air and moisture. Fig. 3.b shows the 2nd parameter that is the separation process of NPS powder from the etchant solution (using filtration process). The polycrystalline spectra of NPS powder is appearing clearly. At the formation of pure SiO_2 the broad spectrum has appeared in case of gaining the powder without separation process. The combinations of two techniques simultaneously produce the compression and the rarefaction cycles of ultrasound waves result in bubble formation. Noticeable, the greatest value of KOH_{conc} produces the smallest value of the crystallite size (27 nm) which corresponds to the largest value of the energy gap (2.05 eV).

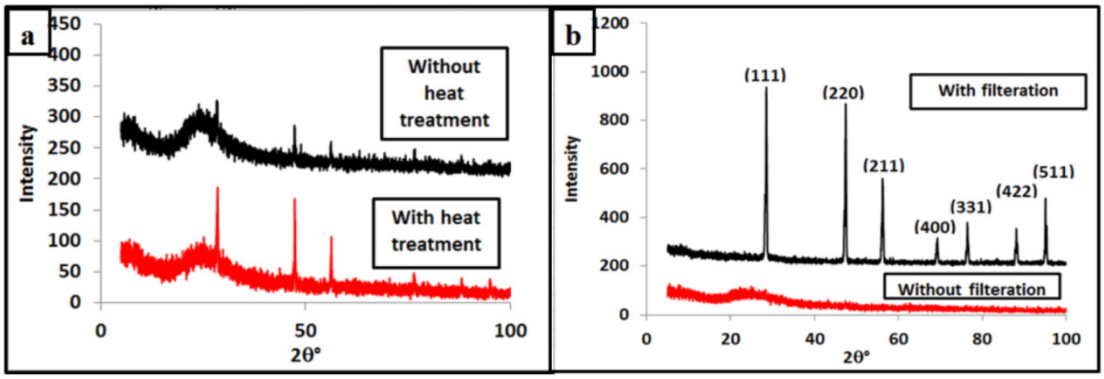

Fig. 3: XRD patterns of NPS and (SiO_2/NPS) powders using at different effective parameters; (a) $KOH_{conc.}$ = 6 wt %, sonication time = 4 hr, at fast and slow drying process. (b) $KOH_{conc.}$ = 4.5 wt %, sonication time = 4 hr, using separation process and without.

Fig. 4 shows the energy dispersive X-ray analysis (EDAX) comparison between the commercial Si powder sample and NPS powder product. The weight percent of Oxygen element is increased by exposing the commercial Si powder to the etching mixture (4.5 wt% KOH and 30 vol% n-propanol) in presence of ultra-sonication waves for 4 hr. The weight percentage of O is 11.77% in case of commercial Si powder, but its value is increased to 56.96% as shown in fig. 4 (after). Then, its argent to know what the chemical bonds are already formed in the product! It was necessary to study the FTIR and Raman spectra of the NPS product.

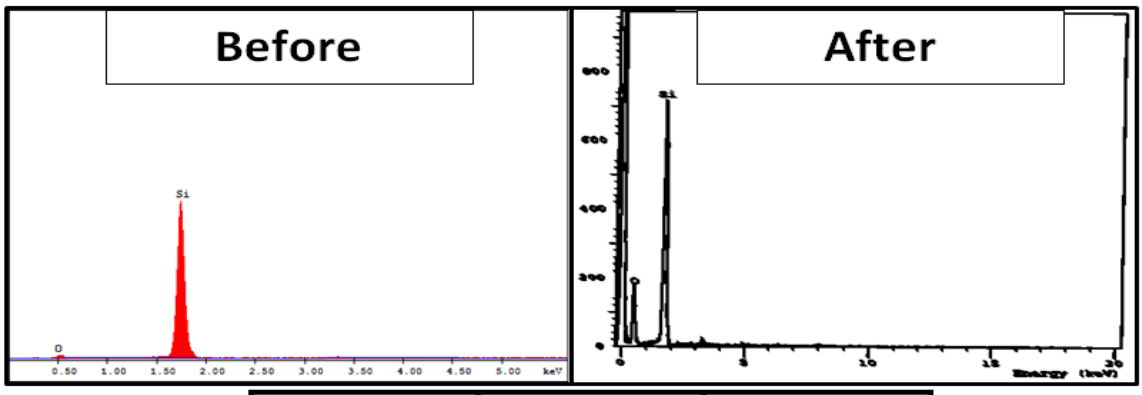

Element	O	Si
Wt % (before)	11.77	88.23
Wt% (after)	56.96	44.07

Fig. 4: EDAX data of commercial Si powder (before) and NPS powder using $KOH_{conc.}$ = 4.5 wt %, 4 hr, and fast-drying (after).

Infrared transmittance analysis reveals information on powders' surface chemistry and how it changes as a function of the sonication times. The FTIR spectrum of the Si-powder after the combination of alkali chemical etching process and the ultra-sonication technique is depicted in Fig. 5. The band in the region (1000–1300) cm^{-1} is assigned to Si–O in the asymmetric stretching in Si–O–Si at different KOH_{conc}. The characteristic bands at 802 and 466 cm^{-1} are corresponding to the stretching and bending vibrational, respectively. The NPS powder is formed that is recorded at wavenumber value 1093 cm^{-1} [8]. The broad band in the range 3050 to 3750 cm^{-1} corresponds to O-H stretching modes in SiOH groups and H_2O, in addition 1637 cm^{-1} due to O-H scissor bending vibration in the water.

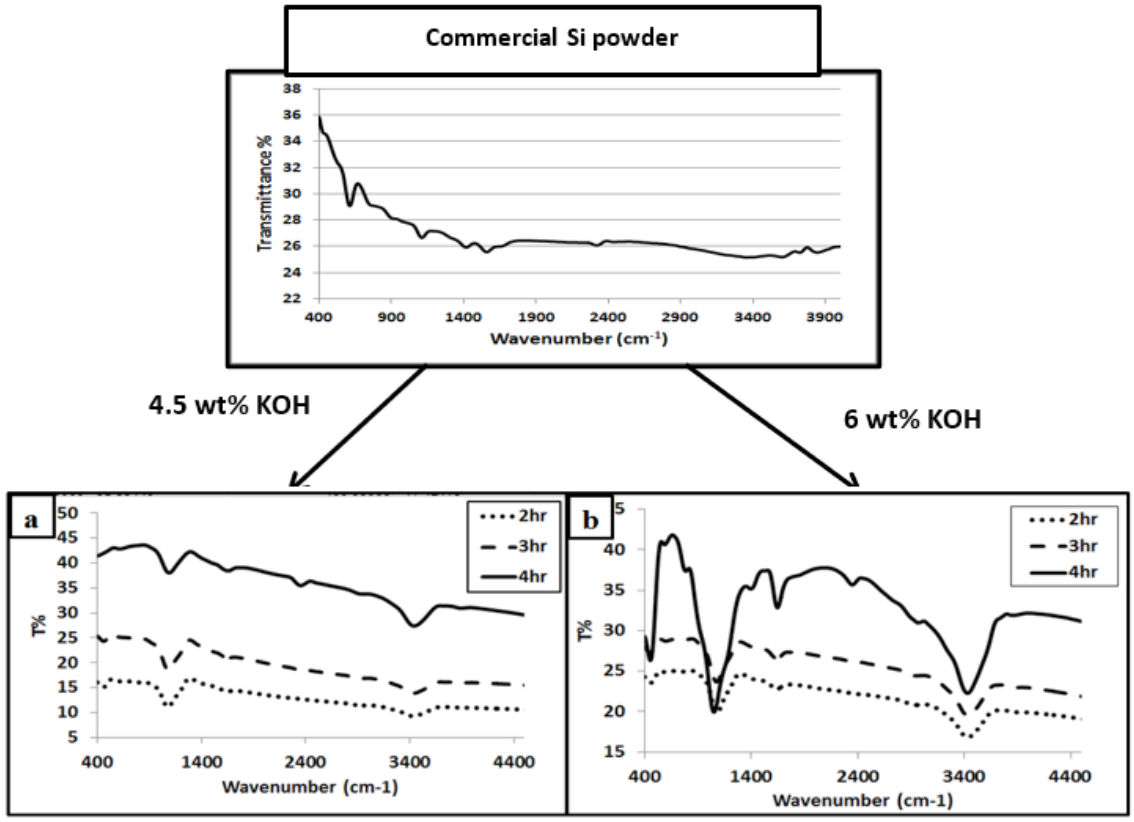

Fig. 5: FTIR spectra of NPS powder at different $KOH_{conc.}$ and sonication times; a) $KOH_{conc.}$ = 4.5 wt %, sonication time = 2, 3 and 4 hr, b) $KOH_{conc.}$ = 6 wt %, sonication time = 2, 3 and 4 hr.

Fig. 2 and 5 proves the agreement of FTIR results and XRD data. The NPS powder is partially formed that appears NPS shoulder peak at 1900 cm^{-1}, as shown in the curve behavior similarity. Then, NPS material is already formed as shown in fig. 5.a. In fig. 5.b, the suitable sonication time for $KOH_{conc.}$ = 6 weight% is 4 hr. The NPS formation conditions have a great importance as recorded in fig. 6. At fast drying process, fig. 6.a shows the NPS spectrum that appears clearly at range 1200-1300 cm^{-1} [24, 25]. But, at the slow rate of drying process, the broad spectrum is appeared at the same region as shown previously. Then, the spectrum of Si–O asymmetric stretching in Si–O–Si is appeared [26]. Therefore, the (SiO_2) is formed, which is in line with fig. 3.a. After filtration process, fig. 6.b shows NPS spectra clearly at range 1200-1300 cm^{-1}. Without filtration process, the broad spectrum is appeared [27]; which is in line with fig. 3.b.

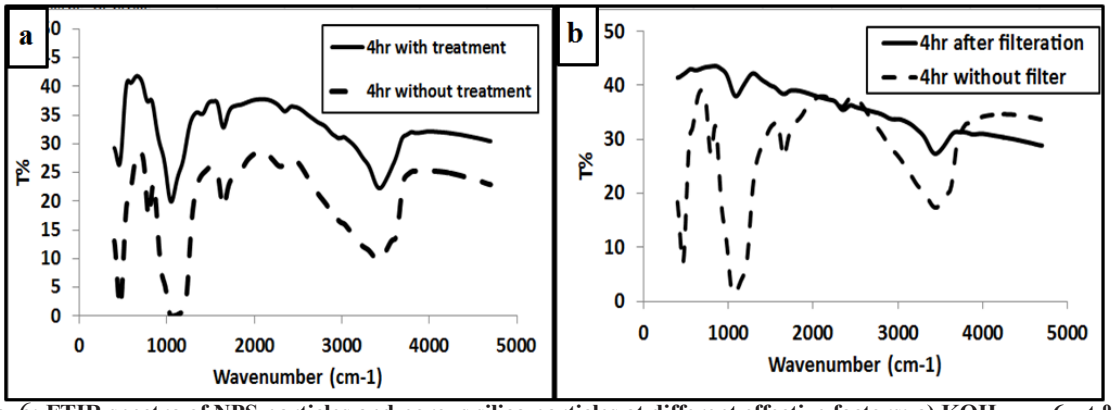

Fig. 6: FTIR spectra of NPS particles and porous silica particles at different effective factors; a) $KOH_{conc.}$ = 6 wt %, sonication time = 4 hr at different drying rate, b) $KOH_{conc.}$ = 4.5 wt %, sonication time = 4 hr using separation process and without.

So, as shown in fig. 5 and fig. 6, the chemical mechanism of the NPS formation can be explained as follows:

$$Si + 2KOH + 2H_2O \rightarrow SiO_2(OH)_2^{-2} + 2K^+ + 2H_2 \quad \text{-----> (1)}$$

$$SiO_2(OH)_2^{-2} + 2K^+ + 2H_2 \rightarrow Si^{\bullet} + 4(OH)^- + 2K^+ + H_2 \quad \text{-----> (2)}$$

$$Si^{\bullet} + 4(OH)^- + 2K^+ + H_2 \rightarrow Si(OH)_4^{\bullet} + 4e^- + 2K^+ + H_2 \quad \text{-----> (3)}$$

$$Si^{\bullet} + 4e^- + 2K^+ + 4H_2O \rightarrow Si^{\bullet} + 2KOH + 2(OH)^- + 2H_2O \quad \text{-----> (4)}$$

In this case, we have obtained the porous silicon, which has the active surface to conduct many chemical reactions, which can be used in many chemical applications that depend on surface chemistry of materials. If the powder is not separated from the oxidation solution used, we will get the silica powder at high pH range (alkaline medium), as shown in the following mechanism:

$$Si^{\bullet} + 2KOH + 2(OH)^- + 2H_2O \rightarrow Si(OH)_4 + OH^- \rightarrow Si(OH)_3O^- + H_2O \text{ -----> (5)}$$

$$Si(OH)_3O^- + Si(OH)_3O^- \rightarrow Si(OH)3\text{-}O\text{-}Si(OH)_3 \text{ -----> (6)} \quad [19]$$

Fig. 7 shows Raman spectra of the synthesized material and exhibits the main typical features of NPS-powder, NPS covered with a SiO_2 layer and pure SiO_2 powder. The shape of the spectra measured for bulk material, it's similar to SiO_2 Raman spectra of literature [27, 28]. After the filtration process, fig. 7.a shows Raman peak spectra at 512 cm^{-1} that corresponds to the presence of Si-O bond [22], at the preparation conditions are $KOH_{conc.}$ = 4.5 wt % at 4 hr. In the case of without separation (filtration process), a weak band at 930 cm^{-1} is observed, in addition to the main peak at 512 cm^{-1}, that appears as a shoulder on the hydroxyl terminated SiO_2 mode (Si-OH) [29]. Then, the NPS powder covered with (SiO_2) layer is observed. Fig. 7.b shows the boson peak with maximum at about 60- 70 cm^{-1} [30], at the preparation conditions $KOH_{conc.}$ = 6 wt % at 4 hr. It's contributed to the main Raman band of bulk material and assigned to scissoring in tetrahedron [$SiO_{4/2}$]. In the region 450– 510 cm^{-1} the Raman modes are essentially Si–Si modes [31]. Fig. 7.b shows several wide bands, which are observed in two cases of drying (fast and slow). The frequencies associated with the vibration modes in the SiO_2 structure at n = 968, 1088 and 1171 cm^{-1} are the transversal, longitudinal and asymmetric stretching, respectively. [32]

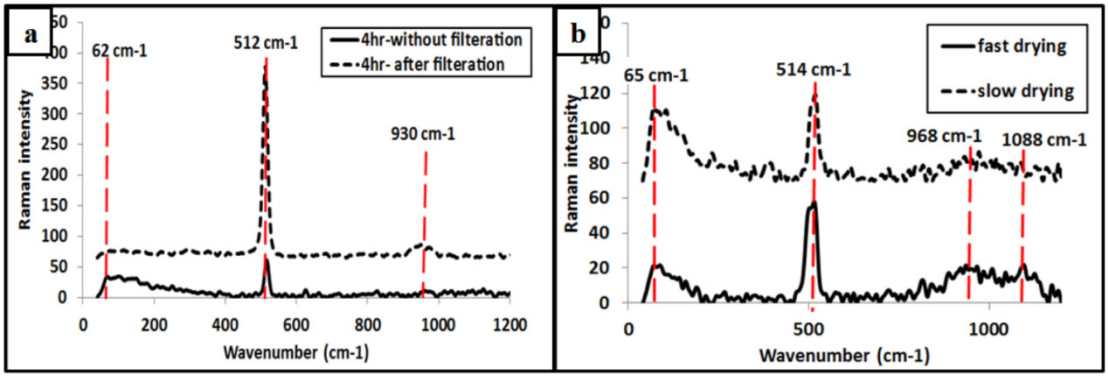

Fig. 7: Raman spectrum of the synthesized materials; a) $KOH_{conc.}$ = 4.5 wt %, sonication time = 4 h, b) $KOH_{conc.}$ = 6 wt %, sonication time = 4 hr.

Fig. 8 shows SEM images of NPS powder product. It clearly shows three different porous architectures, which is as a result of using $KOH_{conc.}$ = 6 wt % at several sonication times. The diameter of NPS rods array is in range (0.634 - 0.894 µm) and its length is ≈ 3.12 µm with a smooth porous surface, as shown in figure 8.a, the pore size is 28-140 nm. At the sonication time enhancement from 2 to 3 hr, it converses the NPS rods array to NPS sheets, so the density of NPS will decrease [33], as shown in Figure 8.b. The lengths of NPS sheets are in range 3.3–9.9 µm. At the sonication time 4 hr, the NPS clusters are observed as shown in figure 8.c, which is more suitable for using in water treatment process (for settle heavy metals, dyes and other mineral) [34]. So, the NPS surface area is more useful than the commercial

silicon powder for many environmental applications [35]; as a removing of different dyes types and heavy metals in wastewater for recycling use.

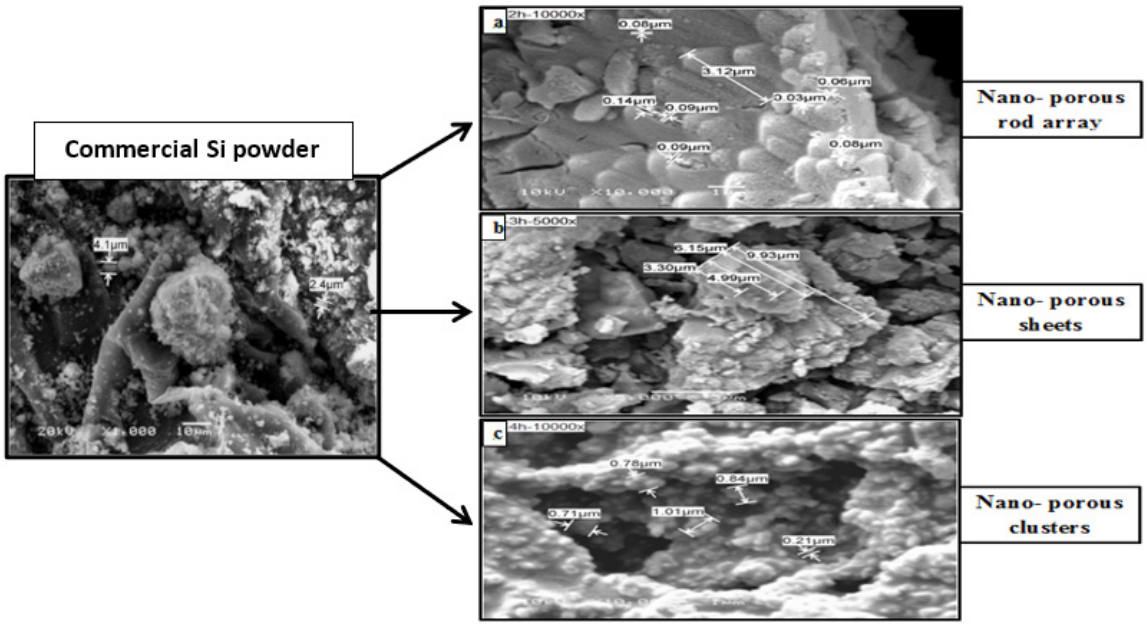

Fig. 8: SEM images of NPS using $KOH_{conc.}$ = 6 wt % at different sonication times; a) 2 hr, b) 3 hr and c) 4 hr.

Fig. 9 shows the TEM images at different magnification, TEM suggest the variation of the NPS surface morphology with exposing to the dual techniques contain the etchant mixture that produces NPS powder. Fig. 9a is an image of the commercial Si powder sample before the sonication process that shows the particle size in range 2-3µm. As for the fig.9b, the image shows the spherical porosity shape of the prepared NPS powder at preparation conditions (6 wt% KOH, at 4hr as sonication time, and fast-drying). So, the same results are obtained that's NPS powder already has been formed.

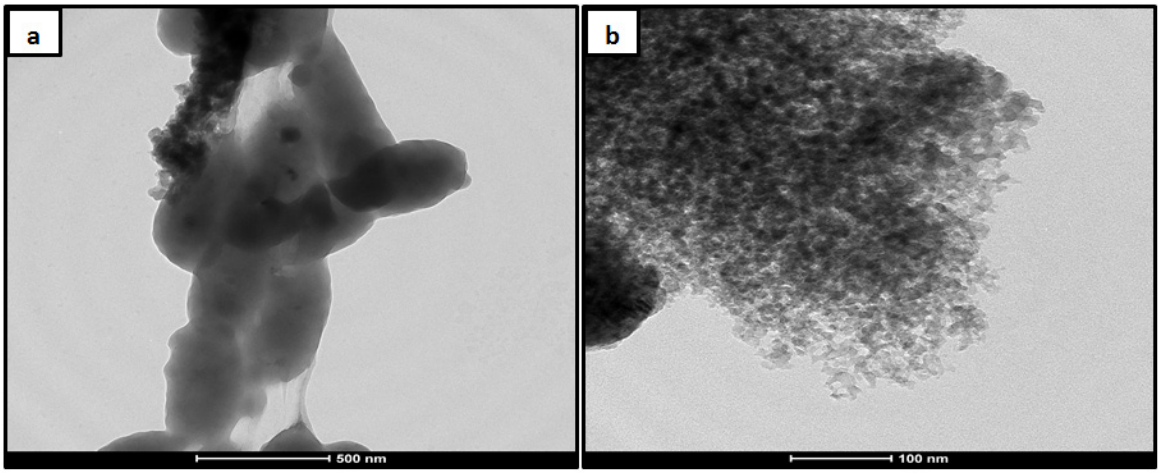

Fig. 9: TEM images a) commercial Si powder, and b) NPS powder using $KOH_{conc.}$ = 6 wt %, 4 hr, and fast-drying.

The heavy metals removal from wastewater is the most suitable application that uses the prepared NPS powder. That's studied in the previous papers [34, 36]

Conclusion

The NPS powder production is the main goal in this study, using combining the alkali chemical etching process and ultra-sonication

technique. It produces improvement of porosity; reducing the cost and enhancing the safety with high yield efficiency. This method is very interesting for the production of NPS powder from metallurgical grade silicon powder. The average crystallite sizes of the samples product are estimated in the nanometer range with several architectures, which are good matches for the values of (crystalline size, pore size and energy gap) and FTIR spectrum. Then, due to using the combined techniques at different conditions, there is a possibility to configure NPS powder; NPS powder coated with (SiO_2) layer and pure (SiO_2) powder, which promotes the use of products in many fields.

References

1. Kashyout A.H., Soliman H.M.A., Nabil M., and Bishara A.A. Impact of congo red dye in nano-porous silicon as pH-sensor. *Sensors and Actuators B*, **216**, 279-285(2015).

2. Kashyout A.H., Soliman H.M.A., Nabil M., and Bishara A.A. Fabrication of congo red/oxidized porous silicon (CR/OPS) pH-sensors. *Material Science and Applications*, **4**, 79-87(2013).

3. Pastor E., Balaguer M., Bychto L., Salonen J., Lehto V.P., Matveeva E., and Chirvony V., Porous silicon for photosensitized formation of singlet oxygen in water and in simulated body fluid: two methods of modification by undecylenic acid. *Journal of Nanoscience and Nanotechnology*, **8**, 1-7(2008).

4. Bespalova K., Somov P.A., and Spivak Y.M., *IOP Conference Series: Journal of Physics Conference Series*, Russian Federation, pp. 012058-012061 (2017).

5. Vinzons L.U., Shu L., Yip S.P., Wong C.Y., Chan L.L.H., and Ho J.C., Unraveling the morphological evolution and etching kinetics of porous silicon nanowires during metal-assisted chemical etching. *Nano Research Letters*, **12**, 385-397(2017).

6. Lytovchenko V.G., Gorbanyuk T.I., Kladko V.P., Sarikov A.V., Safriuk N.V., Fedorenko L.L., Ašmontas S., Gradauskas J., Širmulis E., and Žalys O., Preparation and study of porous Si surfaces obtained using the electrochemical method. *Semiconductor Physics, Quantum Electronics & Optoelectronics,* **20**, 385-395(2017).

7. Saadoun M., Mliki N., Kaabi H., Daoudi K., Bessais B., Ezzaouia H. and Bennaceurab R., Vapour-etching-based porous silicon: a new approach. *Thin Solid Films*, **405**, 29-34(2002).

8. Kashyout A.H., Soliman H.M.A., Nabil M., and Bishara A.A., Fabrication of nano-porous silicon using alkali etching process. *Materials Letters*, **100**, 184-187(2013).

9. Jakubowicz J., Smardz K., and Smardz L., Characterization of porous silicon prepared by powder technology. *Physica E*, 38, 139-143(2007).

10. Manzano F., Fenollosa R., Xifré-Pérez E., Garín M., and Meseguer F., Porous silicon microcavities: synthesis, characterization, and application to photonic barcode devices. *Nanoscale Research Letters*, **7**, 497-502(2012).

11. Khalifa M., Hajji M., and Ezzaouia H., Purification of silicon powder by the formation of thin porous layer followed by photo-thermal annealing. *Nanoscale Research Letters*, **7**, 444-447(2012).

12. Roberts D.S., Estrada D., Yagi N., Anglin E.J., Chan N.A., and Sailor M.J., Preparation of photoluminescent porous silicon nanoparticles by high-pressure microfluidization. *Particle Particle System Characterization*, **34**, 1600326-1600332(2017).

13. Kale P.G., Pratibha S., and Solanki C.S., Synthesis and characterization of Si nanoparticles obtained on sonication of porous silicon multilayer films. *Journal of Nano Research*, **17**, 13-25(2012).

14. Jafari V., Allahverdi A., and Vafaei M., Ultrasound-assisted synthesis of colloidal nanosilica from silica fume: Effect of sonication time on the properties of product. *Advanced Powder Technology*, **25**, 1571-1577(2014). [15]

15. Doktycz S.J., and Suslick K.S., Interparticle collisions driven by ultrasound. *Science*, **247**, 1067-1069(1990).

16. Khan M.N., A-Dwayyan A.S., and Aldalbahi A., Light emitting composite rods based on porous silicon in ormosils and polymer matrices for optical applications. *Optical Laser Technology*, **91**, 203-211(2017).

17. Khalifa M., Atyaoui M., Hajji M., and Ezzaouia H., A new approach to produce porous silicon powder by chemical attack in phase vapor. *European Physical Journal of Applied Physics*, **61**, 30103-30106(2013).

18. Yamada T., Itahara H., and Yamane H., Preparation of micro-porous Si particles from Mg_2Si powder. *Materials Letters*, **98**, 157-160(2013).

19. Nabil M., and Motaweh H.A., Shape Control of Silica Powder Formation. *Journal of Materials Science and Chemical Engineering*, **7**, 49-

55(2019).

20. Kashyout A.H., and Nabil M., Production of high throughput nano-porous silicon (NPS) powder with different architectures. *Materials Chemistry and Physics*, **2016**, 454-549(2018).

21. Russo L., Colangelo F., Cioffi R., Rea I., and Stefano L.D., A mechanochemical approach to porous silicon nanoparticles fabrication. *Materials*, **4**, 1023-1033(2011).

22. Nabil M., Mahmoud K.R., El-Shaer A.H., and Nayber H.A., Preparation of crystalline silica (quartz, cristobalite, and tridymite) and amorphous silica powder (one step). *Journal of Physics and Chemistry of Solids*, **121**, 22-26(2018).

23. Jafarzadeh M., Adnan R., and Mazlan M.K.N., Thermal stability and optical property of ormocers (organically modified ceramics) nanoparticles produced from copolymerization between amino-silanes and tetraethoxysilane. *Journal of Non-Crystalline Solids*, **358**, 2981-2987(2012).

24. Kale P.G., Sharma P., and Solanki C.S., Synthesis and characterization of Si nanoparticles obtained on sonication of porous silicon multilayer films. *Journal of Nano Research*, **17**, 13-25(2012).

25. Nabil M., Elnouby M., Gayeh N., Sakr A.H., and Motaweh H.A., *IOP Confence Series: Materials Science and Engineering*, South Korea, pp. 012001- 012008(2017).

26. López J.A.L., Román A.G., Barojas E.G., Gracia J.F., Juárez J.M., and López J.C., Synthesis of colloidal solutions with silicon nanocrystals from porous silicon. *Nanoscale Research Letters*, **9**, 571-582(2014).

27. Yang L.Y., Li H.Z., Liu J., Sun Z.Q., Tang S.S., and Lei M., Dual yolk-shell structure of carbon and silica-coated silicon for high performance lithium-ion batteries. *Scientific Reports*, **5**, 10908-10917(2015).

28. Borowicz P., Latek M., Rzodkiewicz W., Łaszcz A., Czerwinski A., and Ratajczak J., Deep-ultraviolet Raman investigation of silicon oxide: thin film on silicon substrate versus bulk material. *Advanced Natural Science: Nanoscience and Nanotechnology*, **3**, 045003-045009(2012).

29. Moisii C., Curran M.D., Van-de-Burgt L.J., and Stiegman A.E., Raman spectroscopy of discrete silica supported vanadium oxide: assignment of fundamental stretching modes. *Journal of Material Chemistry*, **15**, 3519-3524(2005).

30. Ivanda M., Clasen R., and Hornfeck M., Raman spectroscopy on SiO_2 glasses sintered from nanosized particles. *Journal of non-crystalline Solids*, **322**, 46-52(2003).

31. Me´ linon P., Ke´ghe´ lian P., Pre´ vel B., Dupuis V., Perez A, Champagnon B., Guyot Y., Pellarin M., Lerme´ J., Broyer M., Rousset J.L. and Deliche`re P., Structural, vibrational, and optical properties of silicon cluster assembled films. *Journal of Chemical Physics*, **108**, 11-18(1998).

32. Spallino L., Vaccaro L., Sciortino L., Agnello S., Buscarino G., Cannas M. and Gelardi F.M., Visible-ultraviolet vibronic emission of silica nanoparticles. *Physical Chemistry Chemical Physics*, **16**, 22028-22034(2014).

33. Ouertani R., Hamdi A., Amri C., Khalifa M., and Ezzaouia H., Formation of silicon nanowire packed films from metallurgical-grade silicon powder using a two-step metal-assisted chemical etching method. *Nanoscale Research Letters*, **9**, 574-584(2014).

34. Nabil M., and Motaweh H.A., *AIP Conference Proceeding*, USA, pp. 020005-020010(2018).

35. Juárez G.S., Barojas E.G., González E.Q., Mora E.S., and López J.A.L., Oxidized porous silicon as a non-interfering support for luminescent dyes. *Mesoporous Biomaterials*, **3**, 61-66(2016).

36. Nabil M., and Motaweh H.A., Dendritic porous silicon as a heavy metal removal (copper element). *Евразийский Союз Ученых (ECV*), **4**, 55-59(2019).

إنتاج السيليكون المسامي (أعواد نانومترية ، صفائح نانومترية ، والتجمعات النانومترية)

مروة نبيل[1]، كمال محمود[2]، رغدة نمير[3]، المغربى المغربى[3]، حسين مطاوع[3]

[1] معهد التكنولوجيا المتقدمة و بحوث المواد الجديدة - مدينة الابحاث العلمية و التطبيقات التكنولوجية - مصر

[2] كلية العلوم- جامعة كفر الشيخ - مصر

[3] كلية العلوم – جامعة دمنهور- مصر

نستعرض فى هذا البحث استخدام تكنولوجيا المساحيق كطريقة رائدة ومنخفضة التكلفة كما انها بسيطة وآمنة لتصنيع مسحوق السيليكون المسامي النانومترى (مسحوق SPN). حيث انها مادة جاذبة للانتباه لاستخدامها في العديد من مجالات البحث. فلقد تم تحضيره باستخدام مزيج من عملية الحفر الكيميائي القاعدى متزامنا مع تقنية الترابط فوق الصوتي ؛ بدءا من خلال مسحوق السيليكون التجاري.فكانت الكفاءة الانتاجية له مبهرة حيث انها وصلت الى (34.18 ٪).

فقد تم تصنيع العديد من الأبنية ثلاثية الأبعاد لمسحوق (SPN) (الآعواد النانومترية sdoronan ، الصفائح النانومترية steehsonan ، والتجمعات النانومترية sretsulconan). فهو عبارة عن مزيج من مسحوق السيليكون المسامي {حجم المسام (82-041 نانومتر)}. كما ثبت أن العوامل الرئيسية التي تؤثر على إنتاج مسحوق SPN هي التركيز الكيميائى لمادة هيدروكسيد البوتاسيوم (cnocHOK) ، الزمن الخاص بعملية الحفر القاعدى، بالاضافة الى عملية الفصل وسرعة التجفيف.